Journal of Applied Polymer Science

Effects of Quasi-3D Stacking Architecture on Interlaminar Shear Strength and Void Content of FRP

Xiaohui Zhang, Yugang Duan, Xinming Zhao, Dichen Li
School of Mechanical Engineering, State Key Laboratory for Manufacturing Systems Engineering, Xi'an Jiaotong University, Xi'an, Shaanxi, 710049, People's Republic of China
Correspondence to: Y. Duan (E-mail: ygduan@mail.xjtu.edu.cn)

ABSTRACT: To improve the interlaminar shear strength (ILSS) of composite laminate, three different quasi-3D stacking architecture (q-3DSA) laminates were fabricated by using automated fiber placement process and a traditional 2D stacking architecture (2DSA) laminate was fabricated as the control sample. The distribution of voids, the density, and the ILSS of four types of laminates were tested. The results indicated that the void content of the different q-3DSA laminates was approximately 0.71%–3.07% greater than that of the 2DSA laminate, but the ILSS of q-3DSA laminates was 5.49%–12.54% better than that of the 2DSA laminate. The microstructure images showed that the cracks spread along the interface between the adjacent layers in the 2DSA laminate, while the cracks cross two or more layers in the q-3DSA laminates. This behavior indicated that the q-3DSA improved the ILSS by dispersing the interlaminar load through the bended and interlaced tows in the laminate. © 2014 Wiley Periodicals, Inc. J. Appl. Polym. Sci. **2014**, *131*, 41076.

KEYWORDS: composites; manufacturing; mechanical properties; properties and characterization

Received 30 March 2014; accepted 29 May 2014
DOI: 10.1002/app.41076

INTRODUCTION

Because of its plentiful advantages of high specific strength and specific stiffness, perdurable resistance to fatigue and corrosion, fiber reinforced plastic (FRP) composites have been widely used in many industrial fields, such as aerospace, energy, and automotive. However, due to the lack of *z*-directions fibers, a major disadvantage of the normal composite laminate is its low through-thickness mechanical properties, particularly the interlaminar shear strength (ILSS).[1–3] Therefore, one of the most important research targets is to enhance the ILSS of FRP. There are two typical methods to improve the ILSS of FRP. One method is to enhance the interface connection performance between the fibers and the matrix, such as matrix modification, fiber treatments, or using nanoparticles and carbon nanotubes to improve the ILSS.[4–8] Another method is to increase the mechanical connection in the thickness direction, such as stitch technology, 3D woven technology, and Z-pins technology.[9–13] Whichever of these methods is used, new manufacturing processes and new equipment need to be developed, and will increase the cost of the composite component.[14]

Automated fiber placement (AFP) is a cost-effective, high-efficiency technology that can manufacture complex composite components for the aerospace and aviation industries.[15–18] Compared with the 3D composite fabrication technologies, the high quality prepreg is one of the very important factors for high ILSS laminates composites in APF process.[19–21] Besides this, the 3D structure can effectively improve the ILSS of composite. But only the traditional composite laminate with 2D stacking architecture can be manufactured by the AFP currently. If composite laminate with 3D stacking architecture is manufactured by AFP, the interlaminar performance of composite laminate will be improved significantly, so will the product efficiency. Nagelsmit et al. have proposed an AP-PLY (Advanced Placed Ply) concept that combines the advantages of fabrics and unidirectional layers in an automated production process. AP-PLY is a laminate configuration obtained by placing the fiber tows in the special patterns mimicking the construction of a woven layer, which can improve the damage tolerance of the composites component.[22] However, few studies have been published concerning the effects of stacking architecture on the ILSS of an AP-PLY laminates. If prepreg tows could be interlaced along the thickness direction of a laminate, it would increase the mechanical connection in that direction. Thereby it would enhance the ILSS efficiently. To verify this hypothesis, a 2D stacking architecture (2DSA) laminate and three different quasi-3D stacking architecture (q-3DSA) laminates were fabricated in this study. The effects of the density, the content of the voids, and the interlaced morphology of different stacking architectures for prepreg plies on the ILSS of these four types of

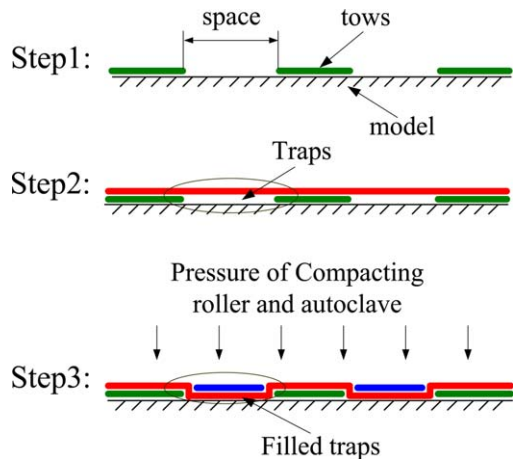

Figure 1. The fabrication schematic diagram of a q-3DSA laminate. [Color figure can be viewed in the online issue, which is available at wileyonlinelibrary.com.]

laminates were studied comparatively. In addition, the possible mechanisms affecting the ILSS were investigated using digital microscope (DM) and scanning electron microscope (SEM).

EXPERIMENTAL

Materials and Equipment

A prepreg, with thickness of 0.13 mm, width of 6.35 ± 0.05 mm, and a resin content of $33 \pm 3\%$, was made of epoxy and carbon fiber (Formosa Plastic Corp. Tairyfil TC35-12K). The fiber placement machine was in-house developed at Xi'an Jiaotong University of China. The manufacturing precision for the composite part is typically under ± 0.5 mm, and the maximum placement speed is 30 m/min. The compacting force varies from 100 to 1500 N, the compacting roller is made by silicon rubber (Shore A hardness 55), the heating temperature varies from 25°C to 200°C, and a total of sixteen 6.35 mm tows can be re-fed, held, cut individually, and heated and compacted on the mold simultaneously.

Fabrication of the Composite Laminates

The fabrication process of the q-3DSA laminate using AFP is shown in Figure 1. First, the traps are set in the space between two adjacent tows when the first layer is being placed down. The width of the space is a tow width. Next, the compacting roller presses the tows of the upper layer into the traps when the second layer is being placed down. This procedure is continuously repeated to make the layers interlace with each other along the thickness direction of the laminate, i.e., the traps are made in the lower layers and are filled by the tows of upper layers under the compacting pressure until all layers of q-3DSA laminate are placed. Subsequently, the laminates are placed into an autoclave to cure. This makes the tows to fill the traps more firmly. Afterwards the q-3DSA laminate specimens are completely fabricated.

Four types of laminates were fabricated according to ASTM D5687 in this study. The description of the fabrication patterns is as follows:

1. The 2DSA laminate [0/±45/90].
   The 2DSA laminates were fabricated according to a conventional orientation angle [0/±45/90], as shown in Figure 2. The numbers correspond to the layer quantities at their positions.
2. The q-3DSA laminate with circulated interlaced plies (CIP) [0/±45/90]
   The fabrication process of the CIP q-3DSA laminate [0/±45/90] is as shown in Figure 3.
3. The q-3DSA laminate with CIP [0/90]
   The difference in the fabrication process between the CIP q-3DSA laminate [0/±45/90] and the laminate [0/90] was the change in the orientation angle. The details of the fabrication process are as shown in Figure 4.
4. The q-3DSA laminate with non-circulated interlaced plies (NCIP) [0/90]
   The difference between CIP and NCIP [0/90] can be observed from Figure 5 that the layer quantities on the positions cannot be uniform at the same time as a result of changing the placement offsetting distance and the orientation angle for the tows, such that an interlaced stacking architecture could be formed throughout the entire laminate.

Tests and Characteristics

The dimensions of the specimens were measured using Vernier calipers, and the specimens were weighed using a METTLER TOLEDO Excellence XP Analytical Balance with a resolution of 0.01 mg to calculate the density of the composites.

A KEYENCE VH-600 DM was used to observe the microstructure of a transverse section of the samples to evaluate the interlaced state of the plies.

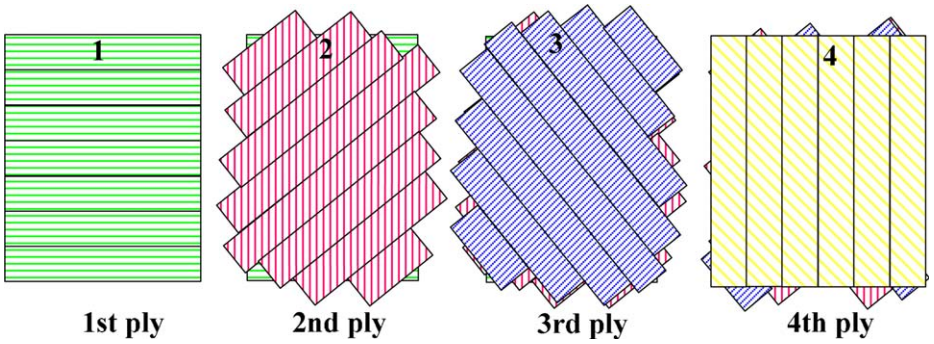

Figure 2. Stacking sequence of the 2DSA laminate [0/±45/90]. [Color figure can be viewed in the online issue, which is available at wileyonlinelibrary.com.]

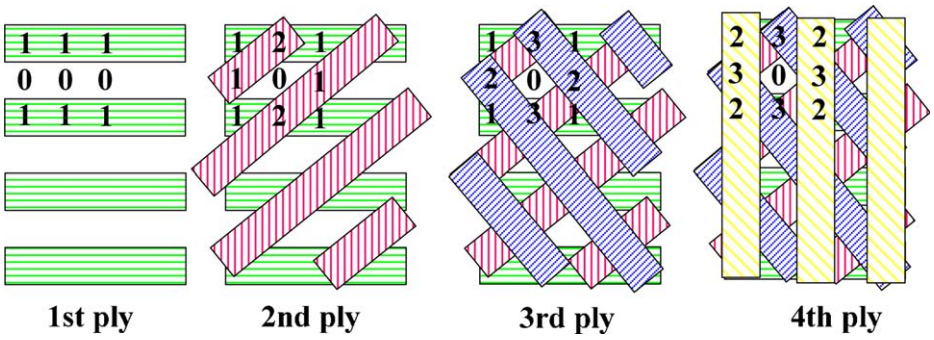

Figure 3. Stacking sequence of the q-3DSA laminate [0/±45/90] for CIP. [Color figure can be viewed in the online issue, which is available at wileyonlinelibrary.com.]

An ultrasonic microscope of SONOSCAN D9500 was used to determine the distribution of voids using a C-SCAN model to assess the distribution of voids of the interlaced plies. The ultrasonic attenuation method was used to measure the voids in the samples according to ASTM E1495-12. The dimension of samples to test the void content was about 150 mm (L) × 100 mm (W) × 6 (Thickness) mm. At first, an energy threshold which can differentiate the void from the composite was determined experimentally using D9500. The energy threshold was 35 (The range is from 0 to 127, the minimum void dimension detected is 0.13 mm, and the probe frequency is 15 MHz.) in this study. And the four planes distributed with the same distance along thickness direction were scanned in the sample, the void content of each plane was determined according to the percentage of the void area to the total scanning area (The software for D9500 was used to calculate the percentage), then the average of void content for the four planes was approximated as the void content of the whole sample.

The ILSS of specimen was tested according to ASTM D2344 using INSTRON 1195, with five samples of each type of laminate. The dimensions of each specimen are 40 mm (L) × 12 mm (W) × 6 mm (thickness).

RESULTS AND DISCUSSION

Effect of the Stacking Architecture on the Density of the Laminates

Figure 6 shows the top (a) and bottom (b) surfaces of a laminate specimen before curing. It can be observed from Figure 6(a) that there are some protrusions on the top surface of the laminate and that the bottom surface is smooth. This observation indicated that the traps in the q-3DSA laminate were not filled completely by the rolling of the compacting roller. Figure 7 shows the top (a) and bottom (b) surfaces of the laminate specimen after being cured in the autoclave. It can be observed from Figure 7(a) that there are some depressions on the top surface and that the bottom surface is smooth and has some traces of resin flow on it. These observations demonstrate that the traps in the laminate were filled more completely under inner heat and pressure in the autoclave; consequently, the tows that filled in these traps will be bounded more tightly in the interlaced architecture construction.

Figure 8 shows the density variation and void content of the four types of stacking architectures of the laminates. It can be seen from Figure 8 that the density is decreased from 1.463 g/mm^3 to 1.435 g/mm^3, while, the void content is increased from 0.71% to 3.07%. The results suggest that the interlaced stacking architecture would reduce the density of the composite laminates. One of the possible reasons for the reduced density is the different void contents in these four layer structures.

Effect of the Stacking Architecture on the Content of the Voids of the Laminates

Figure 9(a–d) shows ultrasonic scanning images for the 2DSA laminate [0/±45/90], the CIP laminate [0/±45/90], the CIP laminate [0/90], and the NCIP laminate [0/90], respectively.

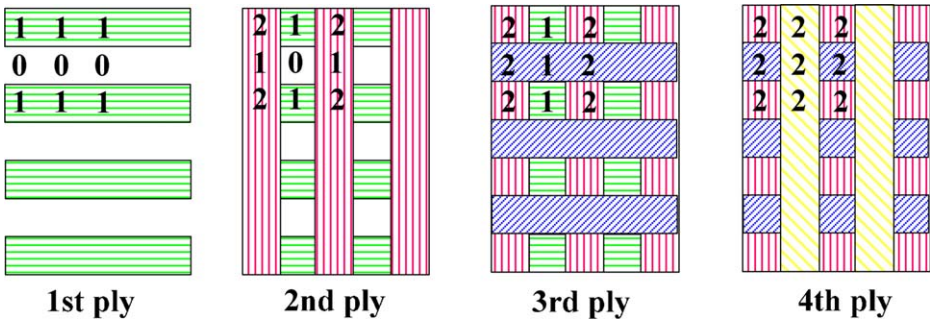

Figure 4. Stacking sequence of the q-3DSA laminate [0/90] for CIP. [Color figure can be viewed in the online issue, which is available at wileyonlinelibrary.com.]

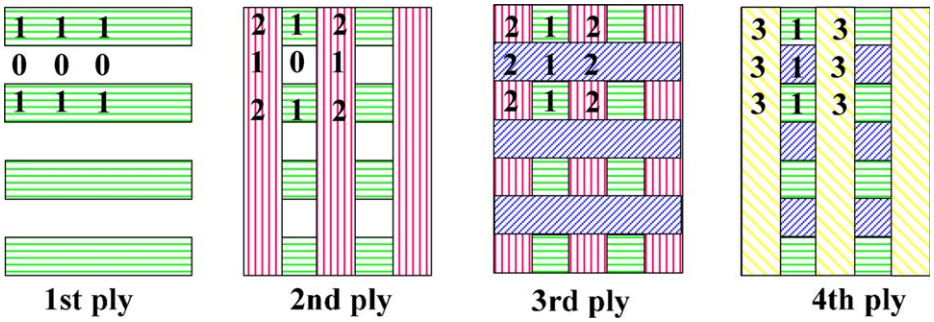

Figure 5. Stacking sequence of the q-3DSA laminate [0/90] for NCIP. [Color figure can be viewed in the online issue, which is available at wileyonlinelibrary.com.]

The white area represents a composite structure, and the black area represents voids in the composite laminate. It can be observed from these pictures that the void content of the 2DSA laminate [0/±45/90] is the minimum and that the void distribution is the most uniform among the four types of laminates. The CIP laminate [0/±45/90], the CIP laminate [0/90], and the NCIP laminate [0/90] all have more voids than the 2DSA laminate [0/±45/90] does. The NCIP laminate [0/90] is found to have the minimized content of void and the most uniform distribution of voids is among the three types of interlaced ply laminates. Moreover, the results of testing the content of void indicate that the density decreased when the void content was increased, and vice versa (as shown in Figure 8).

In Figure 9(b,c), the voids were primarily detected in between two tows and distributed along the direction of the ply angle (as indicated by the arrows). One possible reason for this void distribution could be the effect of the manufacturing precision of the AFP machine. The manufacturing precision of the AFP machine was about ±0.5 mm. This could lead to the reserved gaps on the lower layer were not covered by upper layer tows completely, or the overlapped tows [as shown in Figure 10(a)], then the voids would be formed in the process of AFP. If the voids are not fully filled with flowed resin and deformed fibers in the autoclave curing process [Figure 10(b)], they will be detected by ultrasonic microscope due to the existence of the air. The other possible reason is that the CIP are repeated for each several layers, which resulted in the voids being placed at almost the same projection location on the placement plane in a subsequent process.

Figure 9(d) shows an ultrasonic scanning picture of the laminate using the NCIP stacking structure. The repeatability of the NCIP stacking structure is the poorest. This causes the interlaced plies to be distributed randomly in the laminate, and the q-3DSA to be distributed more uniformly in the laminate.

Effect of Stacking Architecture on the Morphology of Interlaced Plies

The purpose of employing AFP to fabricate q-3DSA laminates is to have the tows interlaced with each other along the thickness direction. Therefore, the observation of a longitudinal section of each of the laminate specimens was used to evaluate the interwoven state among the plies in each of the laminates.

Figure 11(a–d) shows the longitudinal section images for the 2DSA laminate [0/±45/90], the CIP laminate [0/±45/90], the

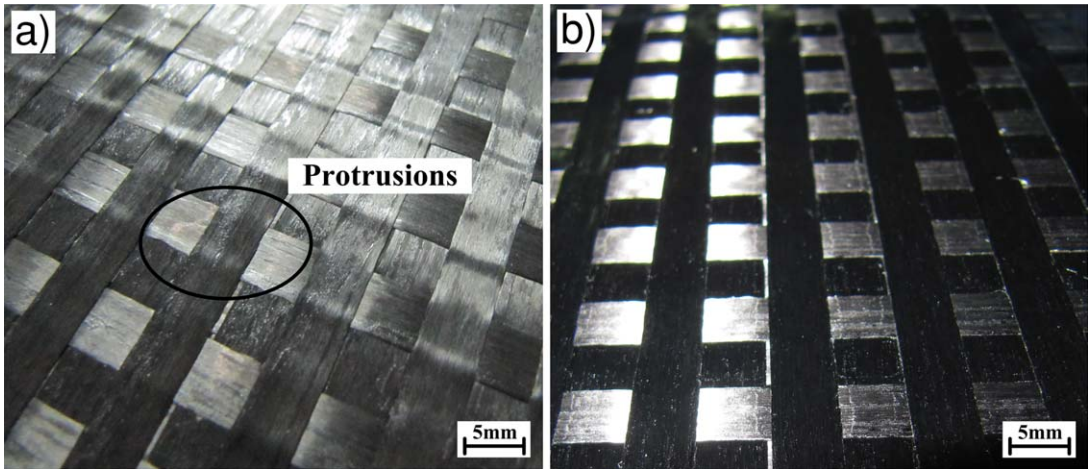

Figure 6. The pictures of composite laminate before autoclave curing: (a) top surface of the laminate, (b) bottom surface of the laminate. [Color figure can be viewed in the online issue, which is available at wileyonlinelibrary.com.]

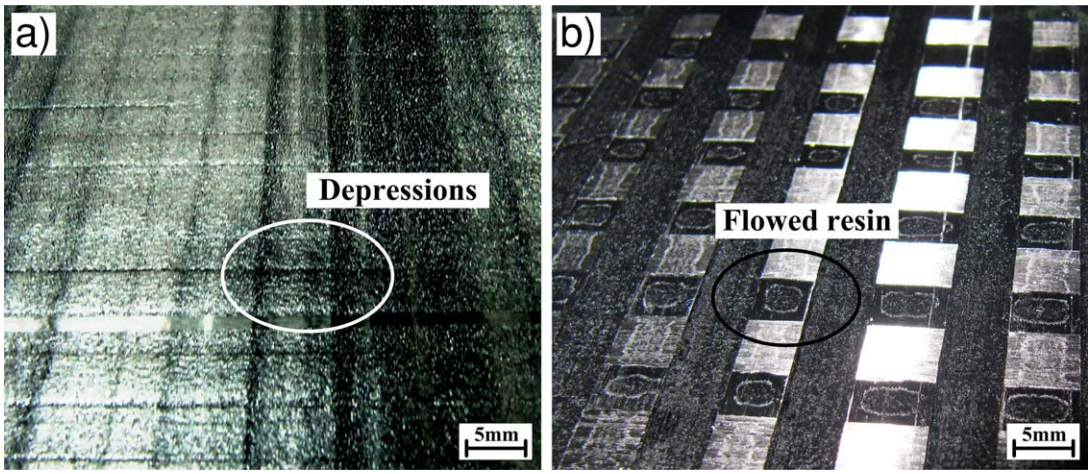

Figure 7. The pictures of composite laminate after autoclave curing: (a) top surface of the laminate, (b) bottom surface of the laminate. [Color figure can be viewed in the online issue, which is available at wileyonlinelibrary.com.]

CIP laminate [0/90], and the NCIP laminate [0/90], respectively. It can be observed from Figure 11(a) that the fibers are typically layered for the 2DSA [0/±45/90] laminate. There are plies with ±45° and 90° between two 0° plies which are straight and have uniform spacing. While, the fibers are bended and interwoven for different extents in the other three q-3DSA laminates [as shown in Figure 11(b–d)], particularly in the NCIP laminate [0/90]. It can be observed from Figure 11(d) that the q-3DSA has been fabricated appropriately because the plies are bended and mutually interlaced.

Effect of the Stacking Architecture on the ILSS of the Laminates

The ILSS of the specimens was tested according to ASTM D2344. Figure 12 shows the ILSS test results for the four types of laminates. It can be noted from Figure 12 that the ILSS of the three q-3DSA laminates are all better than that of the 2DSA laminate. And the ILSS of the CIP [0/±45/90] laminate, the CIP [0/90] laminate, and the NCIP [0/90] laminate is 5.49%, 10.31%, and 12.54% better than that of the 2DSA laminate, respectively.

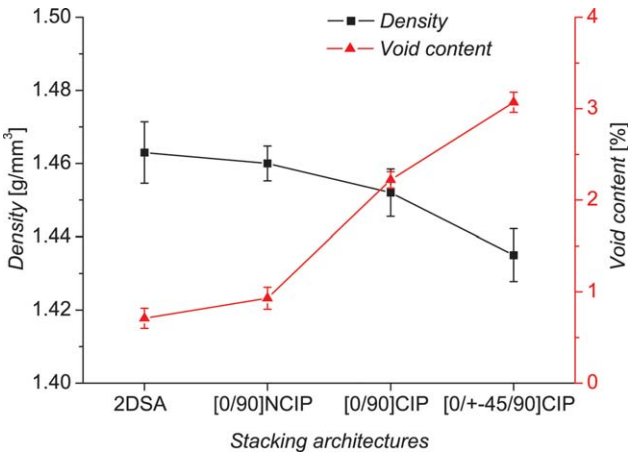

Figure 8. The variations in the density and the void content for the different stacking architecture laminates. [Color figure can be viewed in the online issue, which is available at wileyonlinelibrary.com.]

Figures 13(a,b), 14(a,b), 15(a,b), and 16(a,b) show the longitudinal section DM pictures and SEM pictures of a partial area (as indicated by the circles in the DM pictures) of the 2DSA laminate [0/±45/90], the CIP laminate [0/±45/90], the CIP laminate [0/90], and the NCIP laminate [0/90], respectively. It can be observed from the DM pictures (×60) in Figure 13 that the cracks were generated by the interlaminar shear load after the ILSS tests. Figure 13(a) shows that the cracks in the 2DSA laminate propagate linearly along the fiber direction (indicated as the 0° direction) and that the two cracks between the layers are nearly parallel to each other. However, Figures 14(a), 15(a), and 16(a) show that the cracks in the q-3DSA laminate propagate non-linearly, with the cracks crossing layers along the thickness direction. Figures 13(c), 14(c), 15(c), and 16(c) show the failure section of the whole samples. It can be observed from the pictures that only two adjacent plies bonded with each other in the 2DSA composite laminate, but more than tow adjacent plies cross bonded with each other in the q-3DSA composite laminates.This indicates that interlaminar load can be born by interlaced plies rather than parallel plies in the in the q-3DSA composite laminates.

From the fracture characteristics of the 2DSA laminate and the q-3DSA laminates, the improvements in the ILSS of the composite laminates using q-3DSA can be explained as follows. First, the interlaced and bended tows in the q-3DSA laminates increase the interfacial areas for the same volume of laminate compared to that of 2DSA laminate. Second, the bending interlaced tows are beneficial for passing interlaminar load from one layer to the adjacent layer. These would decrease the shear stress in a certain layer and enable the laminates to bear a higher external load.

Based on the results presented in the Figure 8 and above, although the void content of the q-3DSA laminate is greater

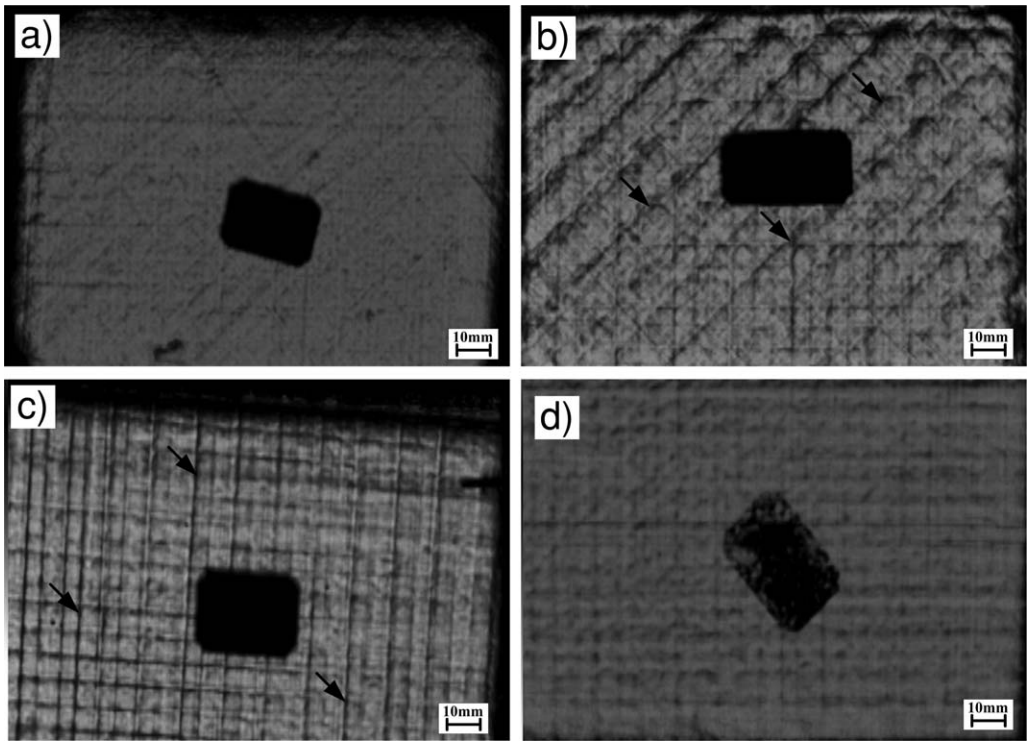

Figure 9. Ultrasonic scanning pictures for different laminates: (a) the 2DSA [0/±45/90] laminate, (b) the CIP [0/±45/90] laminate, (c) the CIP [0/90] laminate, and (d) the NCIP [0/90] laminate.

than that of the 2DSA laminate, the ILSS of the q-3DSA laminate is better than that of the 2DSA laminate. This maybe because the structure of laminates are very different, and the finding indicates that the improvement in the ILSS of the composite laminate caused by the q-3DSA structure is more effective than the decrease in the ILSS induced by the voids resulting from the trap structure. But for the three kinds of q-3DSA structure, the variation of the ILSS is consistent with the literature,[23–25] that is to say, the more voids content, the lower of the ILSS of laminates.

CONCLUSIONS

A fabrication process using AFP technology was used in this study to obtain different types of q-3DSA composite laminates aiming to improve the ILSS of the composite laminate. A traditional 2DSA laminate and three types of q-3DSA laminates were manufactured and tested to evaluate the effects of different stacking architectures on the density, the void content, the interlaced state, and the ILSS of the laminates. The density was slightly affected by the stacking architectures. The change of the void content caused a density variation for the different

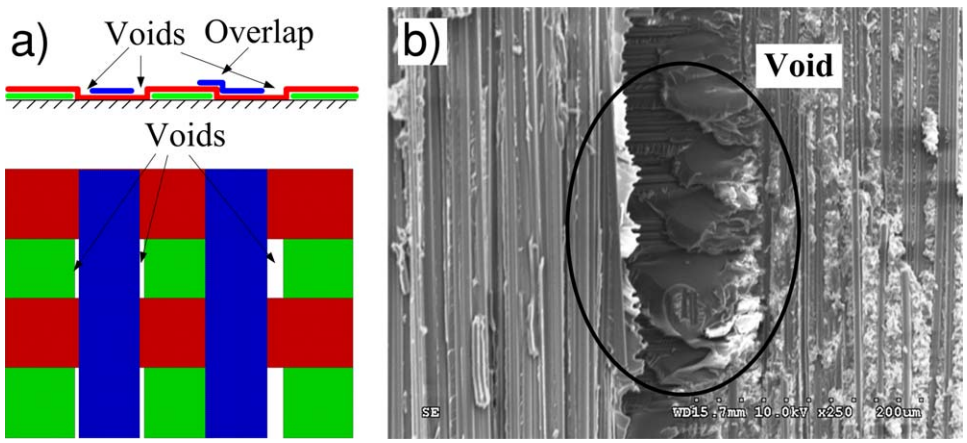

Figure 10. (a) The Schematic diagram of the voids formation and (b) the SEM picture of void. [Color figure can be viewed in the online issue, which is available at wileyonlinelibrary.com.]

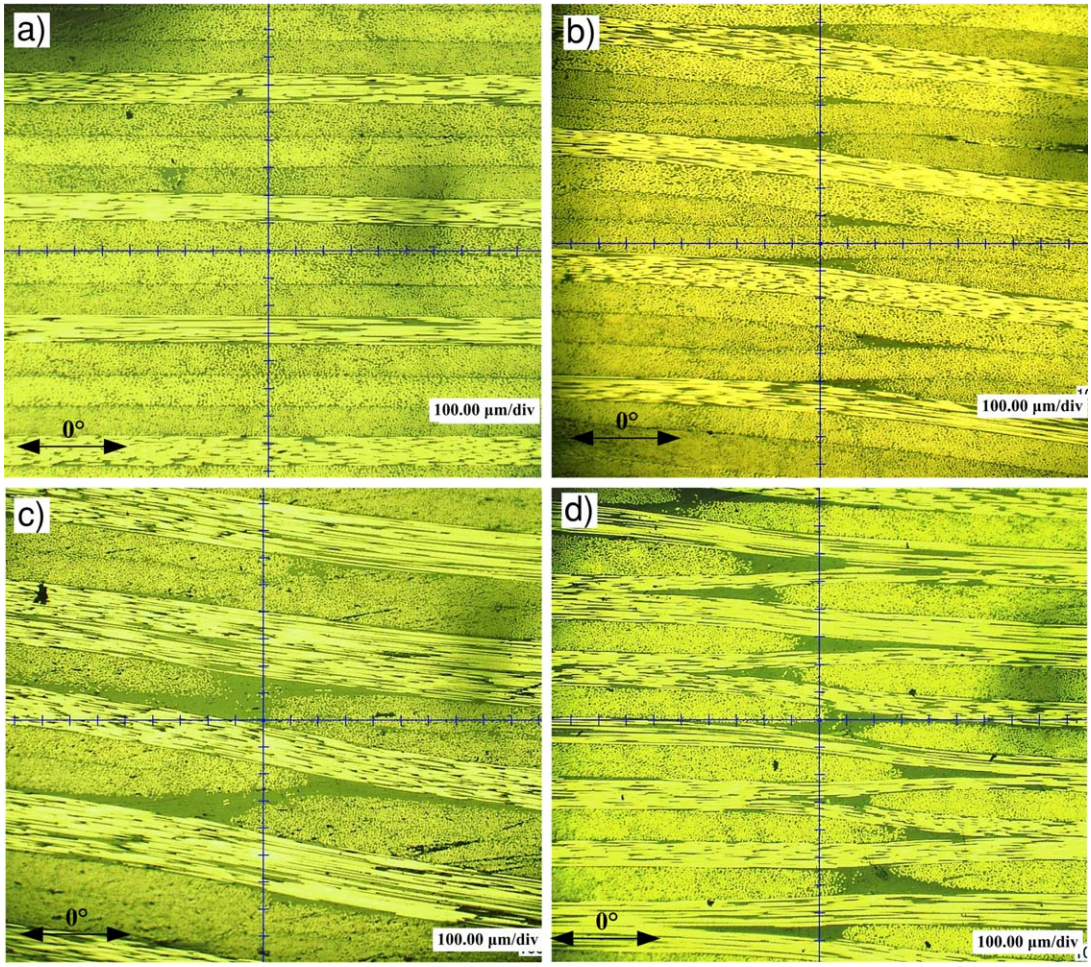

Figure 11. DM pictures of the different laminates: (a) the 2DSA [0/±45/90] laminate, (b) the CIP [0/±45/90] laminate, (c) the CIP [0/90] laminate, and (d) the NCIP [0/90] laminate. [Color figure can be viewed in the online issue, which is available at wileyonlinelibrary.com.]

stacking architectures of the laminates, with more voids resulting in a lower density. This was verified in an ultrasonic imaging test. Moreover, the DM pictures indicate that the q-3DSA enable the tows to deform and, consequently, interlace along the thickness direction. The short beam test results indicate that though the void content of the q-3DSA laminate is approximately 0.71%–3.07% greater than that of the 2DSA laminate, the ILSS of the q-3DSA laminate is still increased 5.49%–12.54% for different types of q-3DSA. This demonstrates that, despite the existence of voids, the q-3DSA can obviously improve the ILSS of composite laminates compared to the 2D laminate and the improvement is superior to the deterioration of the ILSS caused by the voids introduced in the q-3DSA process. The ILSS of the NCIP [0/90] laminate is the highest of the three types of q-3DSA laminates, and its void content is the lowest. This demonstrates that the stacking architecture and void content are two equally effective factors that influencing the ILSS of composite laminates fabricated by AFP. The effects of the q-3D structure on ILSS were studied experimentally in the study. Nevertheless, the further research of effects of the q-3D structure on other properties of composite laminates will be further investigated, as well as theoretical analysis and demonstration of mechanical model for the micro q-3D structure.

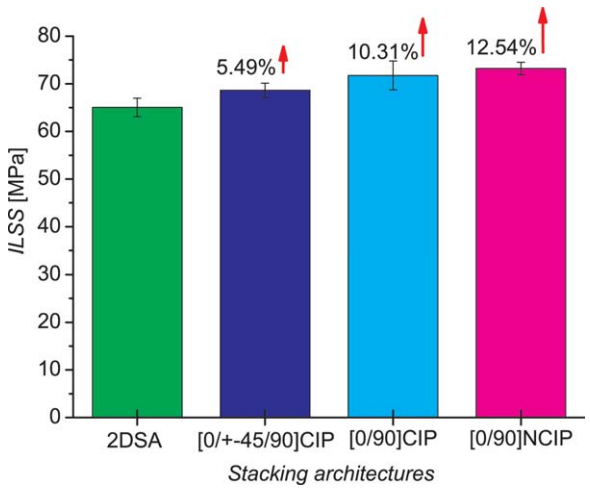

Figure 12. The ILSS of different stacking structure laminates. [Color figure can be viewed in the online issue, which is available at wileyonlinelibrary.com.]

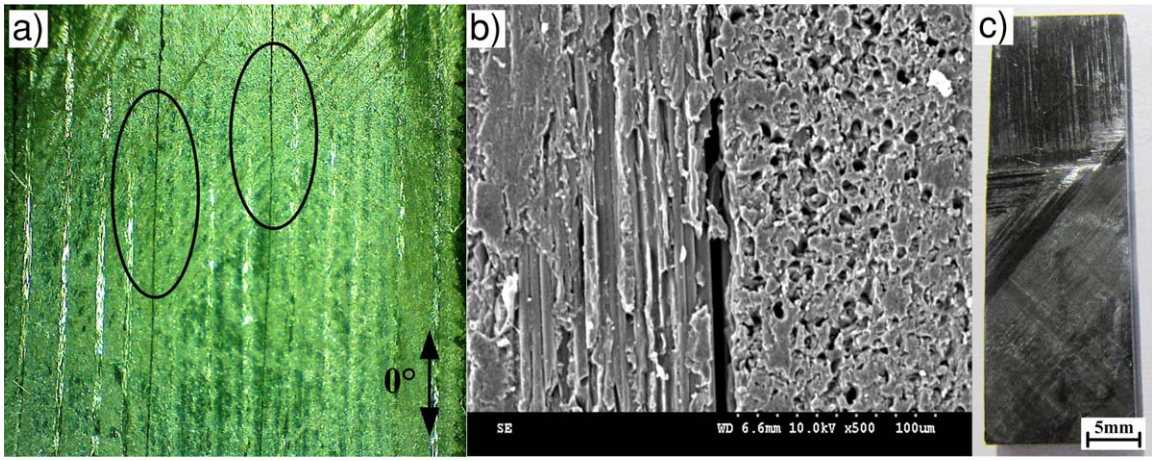

Figure 13. (a) The picture of DM (60×), (b) the picture of SEM, and (c) the interlaminar failure section picture of whole sample for the 2DSA [0/±45/90] laminate. [Color figure can be viewed in the online issue, which is available at wileyonlinelibrary.com.]

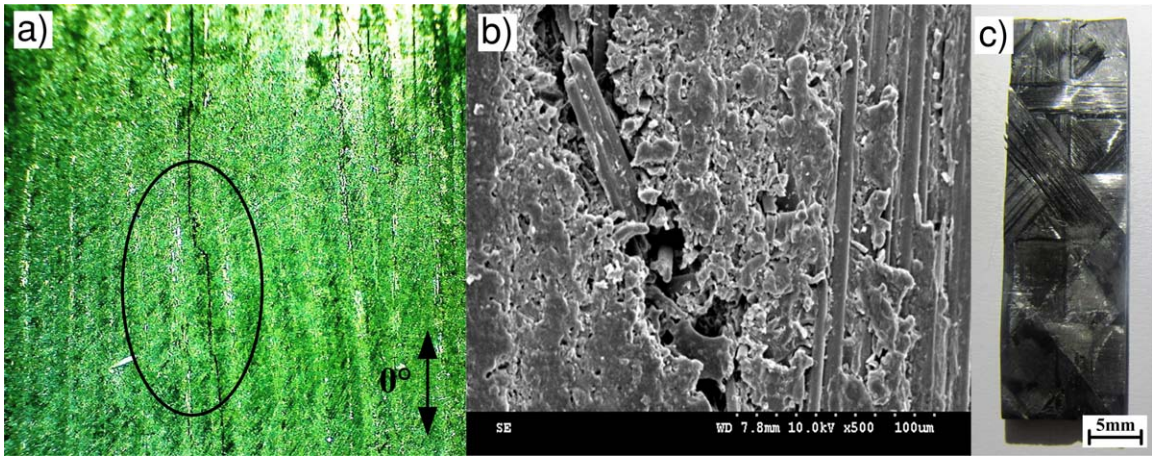

Figure 14. (a) The picture of DM (60×), (b) the picture of SEM, and (c) the interlaminar failure section picture of whole sample for the CIP [0/±45/90] laminate. [Color figure can be viewed in the online issue, which is available at wileyonlinelibrary.com.]

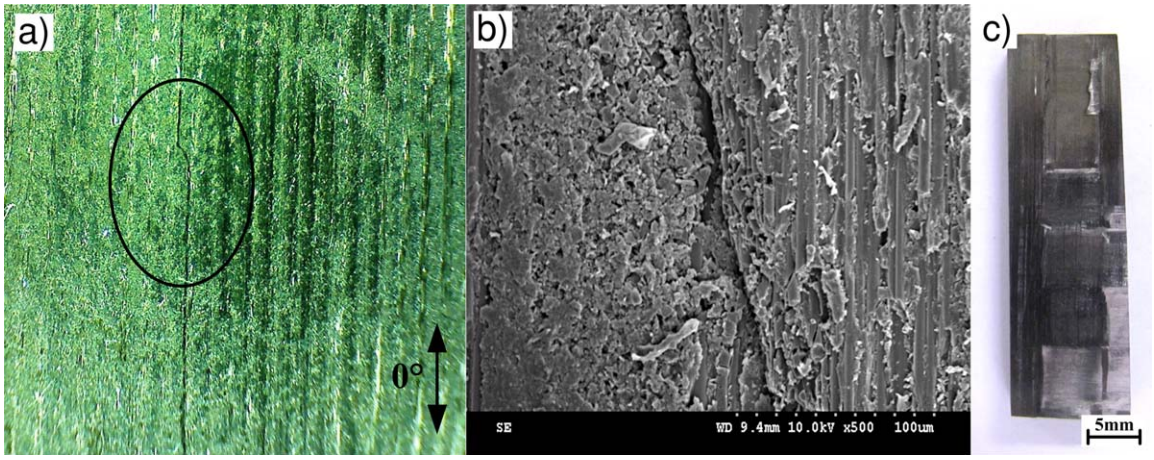

Figure 15. (a) The picture of DM (60×), (b) the picture of SEM, and (c) the interlaminar failure section picture of whole sample for the CIP [0/90] laminate. [Color figure can be viewed in the online issue, which is available at wileyonlinelibrary.com.]

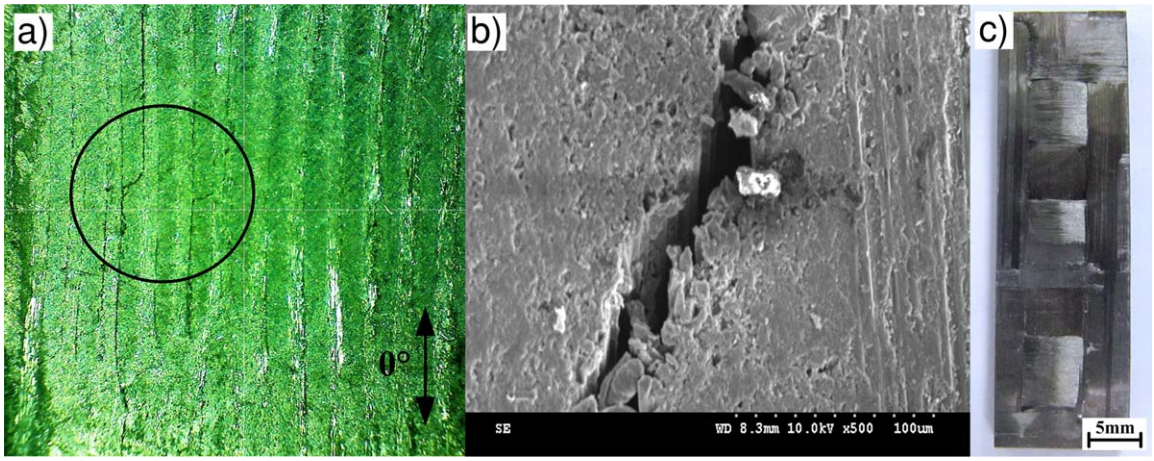

Figure 16. (a) The picture of DM (60×), (b) the picture of SEM, and (c) the interlaminar failure section picture of whole sample for the NCIP [0/90] laminate. [Color figure can be viewed in the online issue, which is available at wileyonlinelibrary.com.]

ACKNOWLEDGMENTS

This research was supported by the NSFC of China [51275393], the Specialized Research Fund for the Doctoral Program of Higher Education [20120201110032], the Program for New Century Excellent Talents in University [NCET-11-0419], and the National High Technology Research and Development Program of China [2012AA040209].

REFERENCES

1. Tong, L.; Mouritz, A. P.; Bannister, M. K. 3D Fibre Reinforced Polymer Composites; Elsevier: Kidlington UK, **2002**, Chapter 1, p 1.
2. Sideridis, E.; Papadopoulos, G. A. *J. Appl. Polym. Sci.* **2004**, *93*, 63.
3. Bryan, H. Engineering Composite Materials; The Institute of Materials: London, **1999**, Chapter 4, p 85.
4. Fan, Z. H.; Santare, M. H.; Advani, S. G. *Compos. Part A* **2008**, *39*, 540.
5. Yu, L.; Jiao-Ping, Y.; Hong-Mei, X. *Compos. Part B* **2012**, *43*, 95.
6. Bozaci, E.; Sever, K.; Sarikanat, M.; Sarikanat, M.; Seki, Y.; Demir, A.; Ozdogan, E.; Tavman, I. *Compos. Part B* **2013**, *45*, 565.
7. Li, W.; Yao, S. Y.; Ma, K. M. *Polym. Compos.* **2013**, *34*, 368.
8. Chandrasekaran, V.; Advani, S. G.; Santare, M. H. *Compos. Part A* **2011**, *42*, 1007.
9. Mouritz, A. P. *Compos. Part A* **2007**, *38*, 2383.
10. Tan, K. T.; Yoshimura, A.; Watanabe, N.; Iwahori, Y.; Ishikawa, T. *Compos. Sci. Technol.* **2013**, *74*, 194.
11. Mouritz, A. P.; Bannister, M. K.; Falzon, P. J.; Leong, K. H. *Compos. Part A* **1999**, *30*, 1445.
12. Cartie, D.; Troulis, M.; Partridge, I. K. *Compos. Sci. Technol.* **2006**, *66*, 855.
13. Bogdanovich, A. E.; Mohamed, M. H. *SAMPE J.* **2009**, *45*, 8.
14. Abali, F.; Pora, A.; Shivakumar, K. *J. Compos. Mater.* **2003**, *37*, 453.
15. Beckwith, S. W. *SAMPE J.* **2013**, *49*, 5.
16. Lukaszewicz, D.; Ward, C.; Potter, K. D. *Compos. Part B* **2012**, *43*, 997.
17. Croft, K.; Lessard, L.; Passini, D. *Compos. Part A* **2011**, *42*, 484.
18. Grant, C. *Ind. Robot.* **2006**, *33*, 117.
19. Nagelsmit, M.; Kassapoglou, C.; Gurdal, Z. *SAMPE J.* **2011**, *47*, 36.
20. Jiang B.; Huang Y. D.; Liu L.; Hu C.P. *J. Appl. Polym. Sci.* **2012**, *125*, 2485.
21. Centea, T.; Hubert, P. *Compos. Sci. Technol.* **2011**, *71*, 593.
22. Jiang, B.; Huang, Y. D. *Compos. Part B* **2011**, *42*, 946.
23. Thomason, J. L. *Composites* **1995**, *26*, 467.
24. Bowles, K. J.; Frimpong, S. *J. Compos. Mater.* **1992**, *26*, 1487.
25. Yoshida, H.; Ogasa, T.; Hayashi, R. *Compos. Sci. Technol.* **1986**, *25*, 3.